The in-depth residual strain heterogeneities due to an indentation and a laser shock peening for Ti-6Al-4V titanium alloy

Q. Xie, R. Li, Y.D. Wang, R. Su, J. Lian, Y. Ren, W. Zheng, X. Zhou, Y. Wang

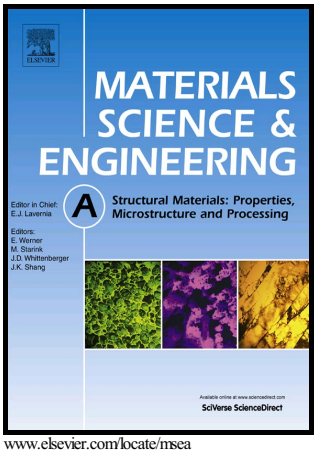

www.elsevier.com/locate/msea

PII: S0921-5093(17)31671-4
DOI: https://doi.org/10.1016/j.msea.2017.12.073
Reference: MSA35915

To appear in: *Materials Science & Engineering A*

Received date: 27 September 2017
Revised date: 17 December 2017
Accepted date: 18 December 2017

Cite this article as: Q. Xie, R. Li, Y.D. Wang, R. Su, J. Lian, Y. Ren, W. Zheng, X. Zhou and Y. Wang, The in-depth residual strain heterogeneities due to an indentation and a laser shock peening for Ti-6Al-4V titanium alloy, *Materials Science & Engineering A,* https://doi.org/10.1016/j.msea.2017.12.073

The in-depth residual strain heterogeneities due to an indentation and a laser shock peening for Ti-6Al-4V titanium alloy

Q. Xie[1], R. Li[1], Y. D. Wang[*,1], R. Su[2], J. Lian[3,*], Y. Ren[4], W. Zheng[1], X. Zhou[5], Y. Wang[6]

1. State Key Laboratory for Advanced Metals and Materials (SKLAMM), University of Science and Technology Beijing, Beijing 100083, China
2. School of Materials Science and Engineering, Beijing Institute of Technology, Beijing 100081, China
3. Steel Institute, RWTH Aachen University, Intzestrasse 1, 52072 Aachen, Germany,
4. X-Ray Science Division, Argonne National Laboratory, Argonne, Illinois 60439, USA
5. Science and Technology on Plasma Dynamics Laboratory, Air Force Engineering University, Xi'an, Shanxi 710038, China
6. Beijing Institute of Aeronautical Materials, Beijing, 100095, China

Abstract

Heterogeneity of the through-thickness residual strain due to the laser shock peening (LSP) process in comparison with that due to the indentation was studied in Ti-6Al-4V alloy samples. The latter is almost a quasi-static process while the former features extremely high strain-rate deformation. The synchrotron based high-energy X-ray diffraction was employed to investigate the through-thickness residual strain distribution. The studied two samples feature almost equal both indentation/peening affected depths (~2 mm) and the maximum magnitude of compressive residual strains (~4000 με) parallel to the surface. The pit depth for the indentation is ~9 times higher than that for the LSP. The position featuring the maximum magnitude of compressive residual strain is in the sub-surface for the indentation while it is in the surface for the LSP. Results of the elastic-visco-plastic finite element simulation for the indentation indicate that the position featuring the maximum plastic deformation corresponds to the maximum magnitude of compressive residual strain. Full width at half maximum (FWHM) of the X-ray diffraction profile can indicate the level of the plastic deformation. It is found that positions with the maximum FWHM indeed correspond to the maximum magnitude of compressive residual strain for both tests.

Key words

Laser shock peening; indentation; Ti-6Al-4V; residual strains; elastic-visco-plastic finite element model.

1. Introduction

Residual strains are typically caused by heterogeneously evolved plastic deformation or thermal mismatch during the manufacturing, welding or joining of

* Correspondence authors: Yan-Dong Wang, e_mail: ydwang@ustb.edu.cn, Junhe Lian, e_mail: Junhe.Lian@iehk.rwth-aachen.de.

metals. 'Residual' here means after the removal of external loads. The residual strain mentioned throughout this paper is elastic type and it is also called residual lattice strain to be different from the residual plastic strain. The elastic type residual strain can be measured by using the X-ray or neutron diffraction techniques and details are described in the following paragraphs. Understanding and controlling the factors that lead to the residual strains is important, since residual strains can impact the mechanical performance and service life of critical engineering components. Compressive residual strains parallel to the sample surface are beneficial when a fatigue crack is potentially propagating along the direction perpendicular to the surface [1]. For heavily deformed metals, the grain-orientation-dependent residual strain may play a very important role in determining the recrystallization texture [2, 3]. Residual strains also lead to the springback of hydro-formed or cold-formed high strength steels [4]. The origin of the back stress [5, 6] can be due to the residual strains, which cause the Bauschinger effect. In industry, residual strains are developed after each processing step, which may result in unexpected stress relaxation or contact stress due to the residual strain. Therefore, it is very important to characterize or predict the residual strain distribution after the plastic deformation and to be able to control it by altering the processing parameters to achieve a reliable design of key engineering components.

Both the indentation and the laser shot peening (LSP) can impose compressive residual strains in the surface. The LSP is a novel technique due to its good preservation of surface roughness, high affected depths and precise impacted position in comparison with the traditional shot peening. As schematically shown in Fig.1, under the high pressure (1~10 GPa), the material yields and plastically deforms with strain rate in a range of 10^6-$10^8 s^{-1}$. At so high strain rates, materials exhibit little change in elastic modulus, but an increase in yield strength [7-9] without the shocked surface being affected thermally [10].

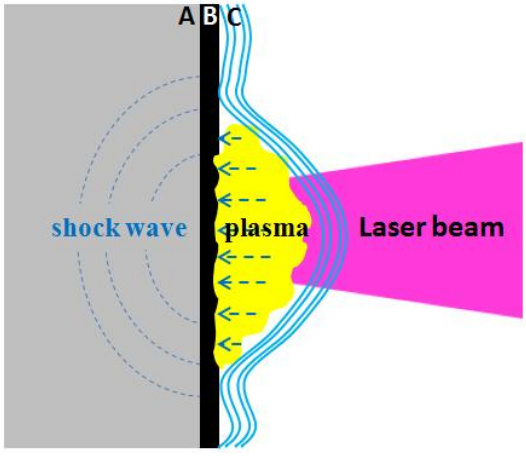

Fig.1 The metallic surface A coated with an overlay B opaque to the laser beam (the laser energy >1 GW/cm^2), above which is a transparent overlay C. The opaque overlay acts as a sacrificial material, a thin layer of which continues to be vaporized and ionized into plasma through absorption of the laser energy. The blow-off of the high temperature plasma can induce a mechanical pressure on

material A. The transparent layer can confine the expansion of the plasma in order to magnify both the magnitude and duration of the pressure in comparison with the condition without the confining layer [11-13].

The process of the LSP is complex, since there exist shock wave reflection and interaction which cause in-depth pressure gradient [14-16]. With the same way as other engineering technique, like the shot peening, introducing the beneficial residual strain in the surface, the LSP utilizes the dynamic mechanical effects of an imparted shock wave to generate a layer of compressive residual strain distributed from the sample surface to the center. Main difference between the traditional shot peening and the LSP lies in the complex dynamic behavior involved in the confined geometry on the engineering component and the complex interaction of elastic and plastic deformation that is governed by the forward and backward wave propagation in the solid for the LSP. On contrary to the LSP featuring an extremely high strain rate, the other extreme case is the quasi-static indentation process with very low strain rate. This paper provides a direct comparison of the influence of variable strain rates due to different processing ways on the multi-scale residual strain distribution. The indentation is easily controlled in experiments and simulated numerically. The level and sign of the residual strain in the specimen after indentation have been investigated in literature [17-21]. But their analysis seldom took the grain orientation distribution in the material into account. The residual strain in titanium alloys is studied in this paper, which is known to have considerable grain-orientation-dependent anisotropy. The grain orientation distribution in the material then can affect both the macroscopic behavior and the residual strain development. Grains featuring different magnitudes and signs of the residual strain can be identified by the synchrotron based high-energy X-ray diffraction.

The present paper aims at gaining an understanding of (1) quantitative difference of the residual strain distribution due to the indentation and the LSP and (2) key factors in controlling the position featuring the maximum magnitude of compressive residual strain and (3) the heterogeneity of the residual strain at grain levels for the two tests. The remainder of the paper is organized as follows. The studied material, the indentation test and the LSP treatment are described in section 2. Details of the employed synchrotron-based high-energy X-ray diffraction technique are also briefly introduced in this section. To estimate the residual strain distribution due to the indentation, the elastic-visco-plastic crystal plasticity finite element model is used in this paper and it is introduced in section 3. Experimental results of the in-depth residual strain profiles from selected families of grains with their specific planes perpendicular to the transverse direction (TD) of the plate are presented in section 4. To understand the experimental data, results from the simulation are provided and discussed in this section. Results of the full-width at half-maximum (FWHM) for different grains measured by the X-ray for the two tests are provided to further understand the results. Section 5 gives some concluding remarks.

2. Experiments

2.1The studied material

A Ti-6Al-4V titanium alloy with a nominal composition of 6.3 Al, 4.17 V, 0.19 Fe, 0.19 O, 0.013 N, 0.0035 H in mass percentage and balanced by titanium is selected as a target material. It is an important material in the aeronautical industry with features of light weight, high strength and good corrosion resistance. The samples were cut from a hot rolled plate and are with dimensions of 100 mm×100 mm×10 mm. They were further annealed for 8 h at 700℃ in nitrogen to relieve the residual stress. The microstructure shows almost equiaxed hexagonal-close-packed (HCP) α-grains and ~15% volume fraction of body-centered-cubic (BCC) β-phase as shown in Fig.2a. The {0002} pole figure of the α-phase measured by the electron backscatter diffraction (EBSD) is given in Fig.2b (the measured area covers more than 50000 grains).

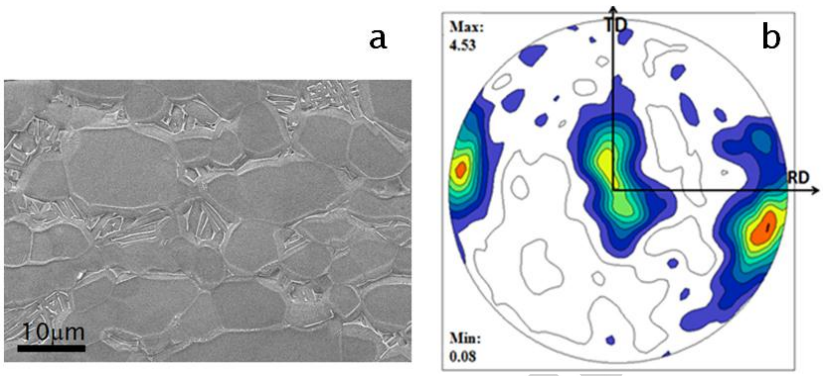

Fig.2 The microstructure of the material after annealing (a) and the {0002} pole figure of the α-phase measured by the EBSD.

2.2 The indentation and the LSP treatments

For the indentation, a Berkovich indenter with a spherical tip diameter of 2.5 mm was used in the test. A vertical force on the indenter was imposed with 150 kg weight. The LSP experiment was carried out with a Nd:YAG pulsed laser operating at a wavelength $\lambda = 1.064$ μm with the pulse duration of 20 ns. The Laser spot diameter is about 3 mm and the laser power density is 7 GW/cm^2. The confining layer and absorbent layer are floating water (1-2 mm thickness) and aluminum foil (0.1 mm thickness) respectively.

2.3 High energy X-ray diffraction to characterize the post indentation/peening material

Transmitted synchrotron X-ray diffraction was performed at the beam-line 11-ID-C, Advanced Photon Source (APS) at Argonne National Laboratory in the USA. A schematic diagram showing the measurement of the residual strain is presented in Fig. 3. One slice of the sample (thickness: 2 mm) after indentation/LSP was cut using the electrical discharging machining. Monochromatic synchrotron X-ray beam with energy 105.22 keV (with a wavelength of 0.11798Å) and beam size 100 μm (height) ×500 μm (width) was used to scan the sample for diffraction pattern collection along the red dashed line as indicated in Fig.3b. The detector was placed at 2 m behind the slice. The lattice strain of different crystallographic planes (ε_{hkil}) is calculated from the change of the measured inter-planar spacing (d_{hkil}) as given in

Eq.(1). The stress-free lattice spacing of each studied lattice plane (d^0_{hkil}) was obtained from one additional X-ray measurement on a sample right after annealing.

$$\varepsilon_{hkil}=(d_{hkil}-d^0_{hkil})/ d^0_{hkil} \quad (1)$$

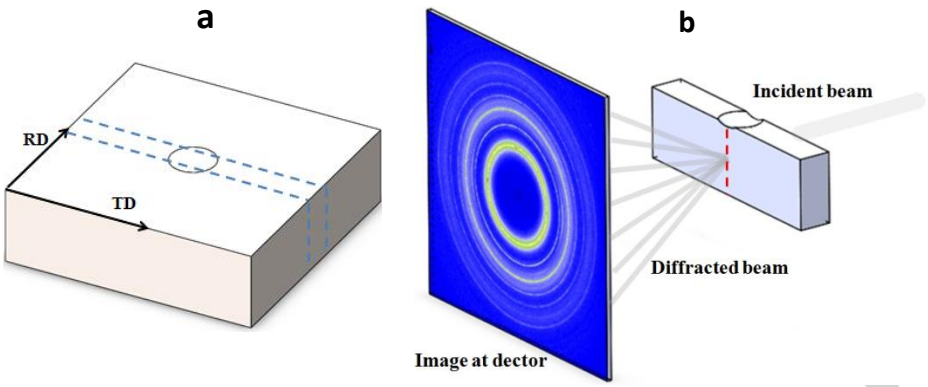

Fig.3 Schematic illustration of the experimental setup for synchrotron X-ray diffraction measurement: (a) the cut position of the slice; (b) the lattice spacing was measured along the red dashed line on the slice.

3. Modeling of the indentation test

An elastic-visco-plastic finite element model (EPFEM) was used to simulate the mechanical behavior of the studied material. Details of the EPFEM were given by Marin and Dawson [22]. The generalized Voce hardening law [23] is used. The finite element method can account for complex boundary conditions and as a result it can be applied to the indentation simulation. The elastic–visco-plastic constitutive relation is incorporated in ABAQUS/Standard by using the user subroutine UMAT. The contact behavior between the rigid spherical indenter and the specimen is assumed frictionless. Displacements of nodes at the bottom of the specimen in the model are constrained to zero in three directions. A penetration displacement of 0.05 mm was applied to the indenter to mimic the indentation process followed by unloading.

Because the indentation affected depth is ~2 mm as will be shown in section 4, a rectangular block with a dimension of 10 mm×10 mm× 3 mm was used and it is meshed into 35070 eight-node brick elements. In order to properly interpret the high plastic deformation gradient right under the indenter, a cylindrical part (highlighted in Fig. 4a) is meshed with very fine resolution. Note also that the FE models have no intrinsic length scale, so dimensions are purely relative. Element type is 3D 8-node continuum element with 8 integration points (C3D8).

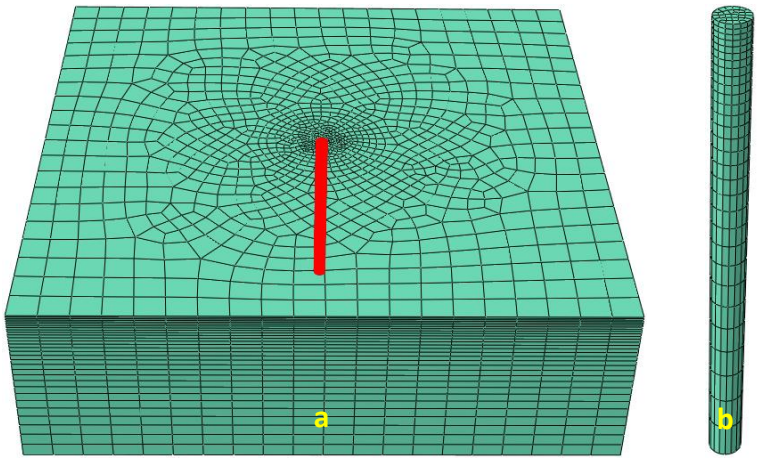

Fig. 4 Geometry of the FE model: (a) a rectangular block with 30 layers of totally 35070 C3D8 elements (diameter of the red cylinder is equal to 0.5 mm); (b) enlarged view of the red cylinder consisting of totally 930 elements (31×30=930).

The β-phase in Ti－6Al－4V was not considered in the model temporarily because of its relatively low volume fraction. Due to the high cost of computation by using the EPFEM, the texture of the material was considered only in the center of the block (the red cylinder in Fig.4a). The other part was modeled as an equivalently isotropic medium. In Fig.4b, there are 496 integration points in each two layers and each integration point in the element represents one grain (eight integration points per element and totally 31 elements per layer and then in total 8×31×2=496 integration points). Totally 496 grains were extracted from the orientation distribution function (ODF) [24] by using the MTEX software [25] as the representative volume element (RVE). Each two layers in the red cylinder is a RVE. After the simulation, the average lattice strain (residual strain studied in this paper) of each two layers in the red cylinder is calculated to output the residual strain distribution through the thickness.

At room temperature, studies in α-Ti have confirmed that dislocation slip can occur on the basal plane {0002}, the prismatic planes {10-10} and the pyramidal planes {10-11} in the close packed <11-20> slip direction. These slip systems cannot provide five independent slip systems to achieve arbitrary imposed deformation. The <a+c> slip systems of {10-11} <11-23> and {11-22} <11-23> are necessary [26]. We omit any deformation occurring due to twinning, since it has been demonstrated that twinning is suppressed in Ti alloys containing Al greater than 4% [27]. The hardening parameters of these slip systems were taken from the same material produced by rolling [28]. The elastic constants are obtained from Ref.[28, 29].

4. Results and discussion

The measured residual lattice strains along the TD (c.f. Fig.3a) after the indentation and the LSP are given in Fig.5.

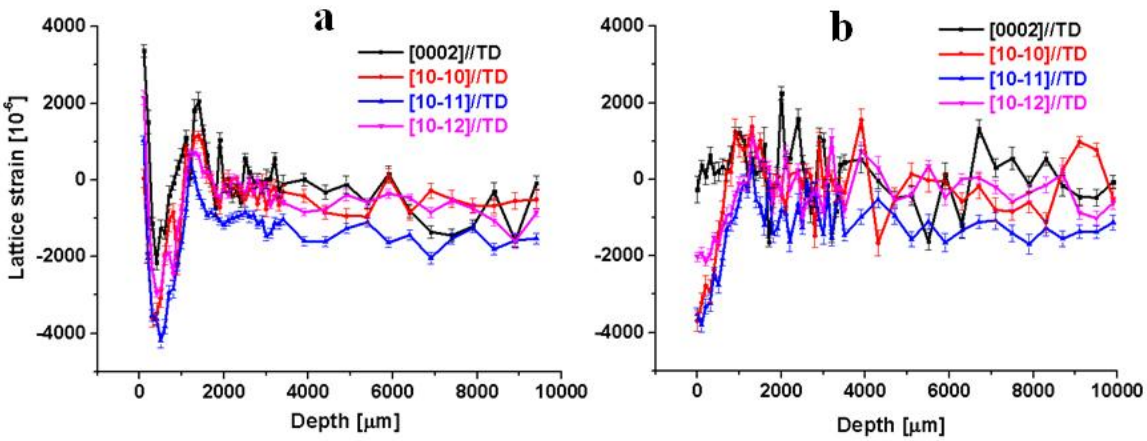

Fig.5 The measured residual strain distribution through the thickness for different lattice planes after the indentation (a) and the LSP (b) respectively. Error bars indicate the standard deviation.

For both tests, the affected depth is ~2 mm and the maximum magnitude of compressive residual strain is ~4000 με. Also, the lattice strain curve from grains with the [0002]//TD is the largest in the affected depth for both tests (tensile strain is positive and compressive strain is negative). At the depth larger than 2 mm, change of the lattice strain is relatively small. The residual strain distribution in the indentation/peening affected depth is very different for different processing procedure. A 'hook' shape of the residual strain profile is obtained after the indentation as shown in Fig.5a. The residual strain in the surface is tensile type. It quickly drops with increasing of the depth and reaches the minimum in the sub-surface (the position with the maximum magnitude of compressive residual strain). With further increase of the depth, the magnitude of the compressive residual strains gradually decreases and it becomes tensile type residual strains at depths larger than 1 mm. They then decrease further with increase in the depth and the lattice strain profiles gradually become flat. Different from that after the indentation, the maximum magnitude of compressive residual strain is in the surface in the sample after the LSP. For both tests, grains with the [0002]//TD feature the largest residual strain and those with the [10-11]//TD almost feature the smallest residual strain. To quantitatively show the measured residual strain in differently oriented grains measured by the X-ray, Table 1 and 2 gives the averaged lattice strain for different grains at different depths for the samples after the indentation and the LSP respectively.

Table.1 The average residual lattice strain [με] for differently oriented grains at different depths after the indentation.

Grain orientations	depth：0-200 μm	depth: 400-600 μm	depth >2000 μm
[0002]//TD	2440	-1600	-315
[10-10]//TD	-936	-2850	-449
[10-11]//TD	-498	-3881	-1285
[10-12]//TD	771	-2618	-492

Table.2 The average residual lattice strain [με] for differently oriented grains at different depths after the LSP.

Grain orientations	depth: 0-200 μm	depth >2000 μm
[0002]//TD	55	11
[10-10]//TD	-3235	-161
[10-11]//TD	-3549	-1069
[10-12]//TD	-2025	-222

The pit profiles after the indentation and the LSP are shown in Fig.6. The pit depth after indentation is ~9 times higher than that after the LSP, i.e. to obtain the same pressure affected depth and the same maximum magnitude of compressive residual strain for the two kinds of procedure, the LSP corresponds to much lower depth of the pit than that due to the indentation. The LSP is good in preserving the surface roughness of the peened material in imposing the compressive residual strain.

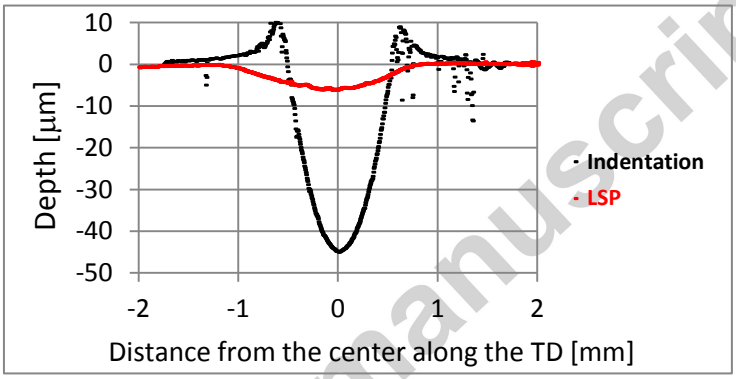

Fig.6 The measured 2D sections of pit profiles after the indentation and the LSP respectively.

To understand the obtained lattice strain profiles, the simulated residual strain distribution after the indentation as a function of depth before and after the unloading is given in Fig.7. Before unloading, the lattice strain in the surface is compressive for all grains. To compensate the compressive strain, the lattice strain at depth of ~1 mm is tensile type and it is the maximum one. Note also that the plastic deformation in the surface is small and it reaches the maximum in the sub-surface. Definition of the accumulative plastic shear, Γ, to indicate the level of the plastic deformation shown in Fig.7 is given in Eq. (2). It gives the accumulative plastic shear of dislocation slip of all involved slip systems during the deformation. Here $\dot{\gamma}^{\alpha}$ is the slip rate of slip system α and the integration is for all of the N slip systems.

$$\Gamma = \int_0^t \sum_{\alpha=1}^{N} \left|\dot{\gamma}^{\alpha}\right| dt \qquad (2)$$

After unloading, release of the lattice strain in the surface is the largest which induces the residual strain in the sub-surface to be more compressive. The maximum

magnitude of compressive residual strain is in the location featuring the maximum plastic deformation. On the other hand, the lattice strain curve from grains with the [0002]//TD is the largest and that for grains with the [10-11]//TD is almost the smallest which agrees with the experimental results obtained from the synchrotron based high-energy X-ray as shown in Fig. 5.

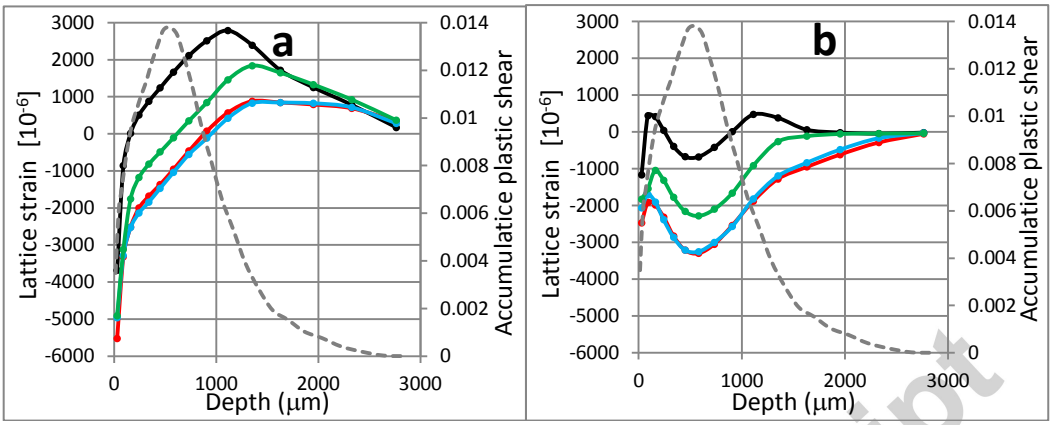

Fig.7 Calculated in-depth lattice strains profile for different grains with their {0002} planes (black solid line), {10-12} planes (red solid line), {10-11} planes (blue solid line), {10-10} planes (green solid line) perpendicular to the TD respectively before (a) and after (b) unloading. The gray dashed line indicates the accumulative plastic shear (averaged values at each depth).

Although the numerical results qualitatively agree well with the experimental findings, the maximum magnitude of compressive residual strain given by the model is somewhat smaller than the experimental values. The reasons could be that (1) the β-phase in the material is neglected in the model and (2) the material parameters are from Ref.[28] instead of for current material. A 'hook' shape lattice strain profile is observed in the predicted ones. A 'hook' shape lattice strain profile after the LSP was reported in Ref.[30]. But in our tests, it was only observed after the indentation. Ref.[9] mentioned that the LSP seldom produces the 'hook' shape residual strain profile in comparison with those observed after the shot peening. Our calculations indicate that the depth with the maximum accumulative plastic shear features the maximum magnitude of compressive residual strains. For the indentation, it is in the sub-surface. Note that the plastic deformation always remains in the material after unloading while the measured residual strain using the X-ray and that studied in the simulation are the elastic type of lattice strain as we mentioned early. The maximum magnitude of compressive residual strain was also observed in the sub-surface for a spherical hard-body impact on a flat surface induced by the shot peening in Ref.[31].

To obtain additional insights into the residual strain behavior for materials after the indentation and the LSP, we plot the in-depth X-ray broadening for both tested samples. It is known that the X-ray diffraction peak broadening is related to several factors [32]. The severity of the plastic deformation can be estimated by observing the diffraction-peak-width changes [32]. The broadening of the full width at half-maximum (FWHM) of the diffraction peak profile is caused by the high

dislocation density, which is proportional to the level of the plastic deformation. We plot the FWHM of grains with their certain planes perpendicular to the TD for both tests, as shown in Fig.8. Indeed, the FWHM is the highest in the surface for the LSP, however, it is the maximum in the sub-surface after the indentation. The FWHM almost does not change at the depth higher than 2 mm. This means that the plastic deformation affected depth for both tests is ~2mm.

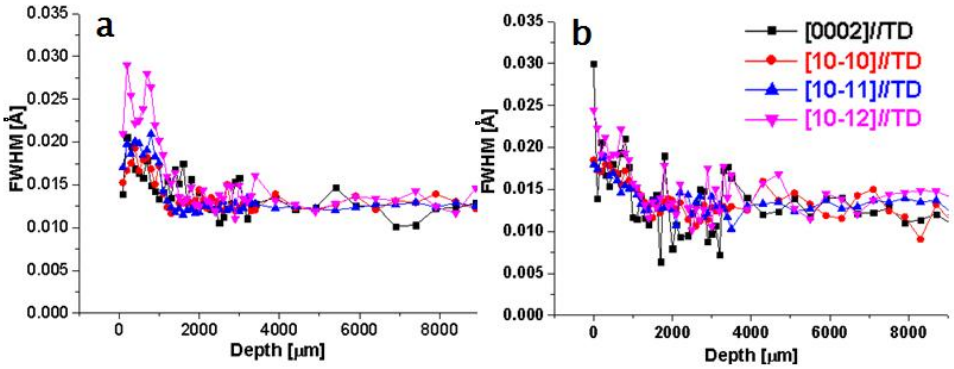

Fig.8 In-depth distribution of the FWHM corresponding to different grains with their {0002}planes (black color), {10-10} planes (red color), {10-11} planes (blue color) and {11-22} planes (pink color) perpendicular to the TD respectively. Results after the indentation is in (a) and those after the LSP is in (b).

5. Conclusions

The in-depth distribution of the residual strains in Ti-6Al-4V alloy after the indentation and the LSP was investigated by the synchrotron based X-ray diffraction technique. A crystal elastic-visco-plastic finite element model was employed to simulate the residual strain distribution after indentation. The following remarks are provided:

(1) In the present study, the indentation and the LSP affected depths are ~2 mm and the maximum magnitude of compressive residual strains are ~4000 με for both processing procedures. However, the pit depth induced by the indentation is ~9 times higher than that by the LSP. The residual strain distribution in the surface generated by the LSP is completely different from that by the indentation. The large compressive strain gradient and the low peened pit depth generated by the LSP certainly benefits for preserving the surface roughness of materials and increasing the fatigue life.

(2) The crystal elastic-visco-plastic finite element simulation indicates that the position featuring the largest plastic deformation corresponds to the maximum magnitude of compressive residual strain after indentation. This was found true for both the LSP and the indentation, concluded from the results by observing the FHHM distribution obtained from the X-ray diffraction. It should be noted that the plastic deformation always remains after unloading, which cannot be directly determined by the well-known diffraction techniques. The studied residual strain is elastic type and it can be measured by the X-ray diffraction by checking the change of the lattice spacing.

(3) The maximum magnitude of compressive residual strain after the LSP is in the surface while that after the indentation is in the sub-surface. The latter corresponds to a 'hook' shape of the lattice strain profile.

(4) The residual strain anisotropy in differently oriented grains was investigated using the X-ray diffraction. Grains with the [0002]//TD feature the largest residual elastic strain in both tests (tensile type residual strain is positive and the compressive one is negative) and that for the [10-11] grains corresponds to the smallest residual elastic strain for both tests. This should be related to the anisotropic behavior of the studied material and can be used for validation of the crystal plasticity modeling for describing the complex grain-to-grain interaction.

Acknowledgement

YDW thanks the financial support from National Science Foundation of China (NSFC) (Grant No.s 51471032 and 51231002), the Fundamental Research Funds for the Central Universities (Grant No. 06111020), and the fundamental research fund at the State Key Laboratory for Advanced Metals and Materials (2014Z-01). QX thanks the financial support from China Postdoctoral Science Foundation (2014M560884), the Fundamental Research Funds for the Central Universities (FRF-TP-14-047A1, FRF-TP-15-057A2) and National Science Foundation of China (NSFC) (Grant No. 51571025).

Reference

[1] B. Denkena, B. Breidenstein, L. Wagner, M. Wollmann, M. Mhaede, Influence of shot peening and laser ablation on residual stress state and phase composition of cemented carbide cutting inserts, Int. J. Refract. Met. H. 36 (2013) 85-89.

[2] Y. B. Park, D. N. Lee, G. Gottstein, The evolution of recrystallization textures in body centred cubic metals, Acta Mater. 46 (1998) 3371-3379.

[3] J. T. Park, J. A. Szpunar, Evolution of re-crystallization texture in non-oriented electrical steels, Acta Mater. 51 (2003) 3037-3051.

[4] J. H. Kim, J. H. Sung, K. Piao, R. H. Wagoner, The shear fracture of dual-phase steel, Int. J. Plasticity 27 (2011) 1658-1676.

[5] X. Feaugas, On the origin of the tensile flow stress in the stainless steel AISI 316L at 300 K: back stress and effective stress, Acta Mater. 47 (1999) 3617-3632.

[6] A. Rao, P. J. Bouchard, S. M. Northover, M. E. Fitzpatrick, Anelasticity in austenitic stainless steel, Acta Mater. 60 (2012) 6851-6861.

[7] J. L. Ocaña, C. Molpeceres, J. A. Porro, G. Gómez, M. Morales, Experimental assessment of the influence of irradiation parameters on surface deformation and residual stresses in laser shock processed metallic alloys, Appl. Surf. Sci. 238 (2004) 501-505.

[8] Y. B. Guo, Laser shock peening (Encyclopedia of Thermal Stresses Editors: Richard B. Hetnarski, 2014, ISBN: 978-94-007-2738-0 (Print) 978-94-007-2739-7 (Online) 2704-2707).

[9] A. H. Clauer, Laser shock peening for fatigue resistance (Surface performance of Titanium, J. K.Gregory, H. J. Rack, D. Eylon (eds.) TMS Warrendale PA, 1996, 217-230).

[10] X. Li, Y. Zhang, J. Chen, Research advance in laser shock processing surface modification technology on metal alloys, Appl. Mech. Mater. 43 (2011) 488-491.
[11] L. Berthe, R. Fabbro, P. Peyre, E. Bartnicki, Wavelength dependent of laser shock-wave generation in the water-confinement regime J. Appl. Phys. 85 (1999) 7552-7555.
[12] J. A. Fox, Effect of water and paint coatings on laser-irradiated targets, Appl. Phys. Let. 24 (1974) 461-464.
[13] W. Zhang, Y. L. Yao, I. C. Noyan, Miceoscale laser shock peening of thin films, part1: experiment, modeling and simulation, J. Manuf. Sci. E.-T ASME 126 (2004) 10-17.
[14] Y. Hu, A. Yao, J. Hu, An analytical model to predict residual stress field induced by laser shock pening, J. Manuf. Sci. E.-T ASME 131 (2009) 031017.
[15] Y. Hu, Z. Yao, Numerical simulation and experimentation of overlapping laser shock processing with symmetry cell, Int. J. Mach. Tool. Manu. 48 (2008) 152-162.
[16] P. Peyre, I. Chaieb, C. Braham, FEM calculation of residual stresses induced by laser shock processing in stainless steels, Modelling Simul. Mater. Sci. Eng. 15 (2007) 205–221.
[17] J. Yan, A. M. Karlsson, X. Chen, Determining plastic properties of a material with residual stress by using conical indentation, Int. J. Solids Struct. 44 (2007) 3720-3737.
[18] X. Chen, J. Yan, A. M. Karlsson, On the determination of residual stress and mechanical properties by indentation, Mater. Sci. Eng A-Struct. 416 (2006) 139–149.
[19] M. Zhao, X. Chen, J. Yan, A. M. Karlsson, Determination of uniaxial residual stress and mechanical properties by instrumented indentation, Acta Mater. 54 (2006) 2823-2832.
[20] S. Suresh, A. E. Giannakopoulos, A new method for estimating residual stresses by instrumented sharp indentation, Acta Mater. 46 (1998) 5755-5767.
[21] B. Clausen, M. B. Prime, S. Kabra, D. W. Brown, Residual stress and plastic anisotropy in indented 2024-T351 Aluminum disks, Proceedings of the SEM annual conference, June 1-4, 2009, Albuquerque New Mexico USA.
[22] E. B. Marin, P. R. Dawson, On modeling the elastic-plastic response of polycrystalline materials, Comput. Meth. Appl. Mech. Eng. 132 (1998) 1-21.
[23] C. N. Tomé, G. R. Canova, U. F. Kocks, N. Christodoulou, J. J. Jonas, The relation between macroscopic and microscopic strain hardening in F.C.C. polycrystals, Acta Metall. Mater. 32 (1984) 1637-1653.
[24] H. J. Bunge, Texture analysis in materials science: Mathematical methods, 1982 (London Butterworth).
[25] F. Bachmann, R. Hielscher, H. Schaeben, Texture Analysis with MTEX - Free and Open Source Software Toolbox, Solid State Phenom. 160 (2010) 63-68.
[26] V. Hasija, S. Ghosh, M. J. Mills, D. S. Joseph, Deformation and creep modeling in polycrystalline Ti-6Al alloys, Acta Mater. 51 (2003) 4533-4549.
[27] A. Fitzner, D. G. L. Prakash, J. Q. Fonseca, M. Preuss, M. Thomas, S. Zhang, J. Kelleher, The Effect of aluminium on deformation and twinning in alpha titanium: the 45º case, Mater. Sci. Forum 765 (2013) 549-553.

[28] A. M. Stapleton, S. L. Raghunathan, I. Bantounas, H. J. Stone, T. C. Lindley, D. Dye, Evolution of lattice strain in Ti-6Al-4V during tensile loading at room temperature, Acta Mater. 56 (2008) 6186-6196.

[29] W. Petry, A. Heiming, J. Trampenau, M. Alba, C. Herzig, H. R. Schrober, G. Vogl, Phonon dispersion of the bcc phase of group-IV metals. I. bcc titanium, Phys. Rev. B 43 (1991) 10933-10947.

[30] A. M. Korsunsky, J. Liu, D. Laundy, M. Golshan, K. Kim, Residual elastic strain due to laser shock peening: synchrotron diffraction measurement, J. Strain Analysis. 41 (2006) 113-120.

[31] B. L. Boyce, X. Chen, J. W. Hutchinson, R. O. Ritchie, The residual stress state due to a spherical hard-body impact, Mech. Mater. 33 (2001) 441-454.

[32] T. Ungar, Dislocation densities, arrangements and character from X-ray diffraction experiments, Mater. Sci. Eng A-Struct. 309–310 (2001) 14-22.